Strain effects on the electronic structure of strongly coupled self-assembled InAs/GaAs quantum dots: Tight-binding approach

W. Jaskólski and M. Zieliński*

Instytut Fizyki UMK, Grudziądzka 5, 87-100 Toruń, Poland

Garnett W. Bryant

National Institute of Standards and Technology, Gaithersburg, Maryland 20899-8423, USA

J. Aizpurua

Donostia International Physics Center, Paseo Manuel Lardizabal 4, 20018 San Sebastián, Spain

We present an atomistic tight-binding study of the electronic structure and optical properties of vertically stacked, double, self-assembled, InAs/GaAs quantum dots. The investigated dots are lens-shaped and are situated on wetting layers. We study coupling and strain effects for closely spaced dots. For intermediate separation distances between the dots, the tight-binding theory confirms the effect of strain-induced localization of the ground hole state in the lower dot, as predicted in other approaches. However, the tight-binding calculations predict weaker localization at large separation distances and no localization for closely spaced and overlapping dots, which have not been investigated so far. An anomalous reversal of the bonding character of the ground hole state for large separation distances, found previously by us for unstrained systems, is present also for strained dots. We also show that in double quantum dots there may exist bound and localized electron and hole states with energies above the edge of the wetting layer continuum. The calculated redshift of the lowest optical transition for decreasing distance between the interacting dots agrees qualitatively with experimental data.

I. INTRODUCTION

Many systems of closely spaced quantum dots (QD) can now be made. Close packed arrays or clusters of quantum dots can be formed from chemically synthesized colloidal nanocrystals.[1–3] Double, quasi-two-dimensional quantum dots, electrically defined in a pair of narrow quantum wells separated by a tunnel barrier, are commonly used to study transport properties of zero-dimensional structures.[4,5] Strongly coupled systems appear also in self-assembled quantum dots as neighbor islands grown in the same wetting layer (WL), or in a vertical stack of closely spaced layers of dots.[6] The later are of special interest because of their applications as quantum dot lasers[6,7] and as qubits for quantum information processing.[8–12] The performance of quantum dot lasers can be enhanced if many layers of self-assembled dots are employed in such devices. However, when the layers are closely spaced, the coupling between quantum dots can affect the structure of optically active transitions, as happens for close packed arrays of chemically synthesized nanocrystals.[2,3,13–15]

Strain due to the lattice mismatch at the interfaces between two semiconductors is the driving force for the growth of self-assembled quantum dots and is known to play an important role in determining the electronic and optical properties of single and multiple self-assembled quantum dots.[16–18] A large number of theoretical works have been devoted to the study of such systems. Atomistic approaches taking strain effects into account have been applied mainly to single quantum dots,[19–23] while coupled dots have been treated usually by simplified, continuous-medium

models.[18,24] Only recently, coupled and strained dots have been investigated in the framework of the pseudopotential approach.[9,25,26]

Here we use an empirical tight-binding formalism (ETB) to investigate the electronic structure and optical properties of lens-shaped, InAs/GaAs self-assembled, vertically stacked, double quantum dots (DQD) situated on 2 monolayer (ML) thick wetting layers. The thickness d of the GaAs spacer layer that separates the top of the lower quantum dot from the bottom of the upper WL varies from 16 ML down to −2 ML (where the upper WL overlaps with the lower QD by 2 ML). Such strongly coupled dots have not been investigated so far. The main aim of this paper is to study strain effects in closely spaced dots in a vertical stack.

II. CALCULATION OF ELECTRONIC STRUCTURE

To calculate electronic states of self-assembled stacked QDs using an atomistic tight-binding approach with strain minimization, we proceed in three steps.

Definition of the structure

First, a system of lens-shaped InAs quantum dots is defined and embedded in a big box of the barrier material (GaAs), which we refer to as the buffer.[21] Initially, all atoms are placed at the lattice sites of a uniform, bulk GaAs zinc-blend lattice. To preserve the axial symmetry of the QDs, we model the external GaAs buffer surrounding the QDs as a cylinder (see Fig. 6). The height of the lenses is $h=3a$ and the base diameter is $D=12a$, where a is the GaAs lattice

constant, $a_{GaAs}=0.5653$ nm. This corresponds to $h \approx 1.8$ nm and $D \approx 7$ nm, which are the smallest sizes attainable in Stransky-Krastanov growth.[14,27] The quantum dots are situated on wetting layers, which are $1a$ (2ML) thick and parallel to the x, y plane (the DQD is made from identical dots aligned one on top of the other). The centers of the quantum dot bases are anion (As) atoms.[28] There are 1397 atoms in a single lens (not counting the WL). It is reasonable to assume that far from the QDs, the GaAa buffer is unstrained. However, the InAs WL and QDs are strongly strained due to the huge strain energy of the compressed InAs WL and QDs, which have an unstrained bulk lattice constant a_{InAs} $=0.6055$ nm.

Strain minimization

In the second step, the strain energy is minimized and the lattice is relaxed to find new positions for the atoms. The effects of strain are calculated by means of the valence force field method (VFF).[17,23] The atomic elastic constants for InAs and GaAs, which appear in the formula for the strain energy in the VFF model, are taken from Ref. 17.

Because strain is a long-range effect, the GaAs buffer used in the strain energy minimization (referred to here as the VFF domain) must be large enough to ensure that the strain fields vanish at the GaAs buffer boundaries. Lee *et al.*[21] investigated in detail the vertical size of the GaAs buffer needed to obtain vanishing hydrostatic strain at the box boundaries. For the lens-shaped InAs QD with $h=3$ nm and $D=15$ nm considered by Lee, the thickness of the GaAs buffer needed above or below the dot was 15 nm, i.e., $26a$. In our calculations of the strain field, we use similar a thickness for the GaAs buffer regions. Thus, for example, for two dots separated by $d=8a$, the height of the entire GaAs cylinder is $H=64a$ (≈ 38.5 nm), the same as its diameter. The entire structure has 1 757 097 atoms. Further increase of the VFF buffer does not change the strain distribution in the area of quantum dot or the final energy spectra. We observe that such a big buffer assures that hydrostatic strain (the trace of the strain tensor) at the buffer edge is 100 times smaller than the large strain in the QD and at the InAs/GaAs interface.

The minimization of the strain energy (lattice relaxation) is performed using a combination of the steepest descent and the conjugate gradient methods.[29] The minimization process stops when the maximum force applied to each atom is <6 $\times 10^{-6}$ eV/nm. Finally the local strain tensor and strain profiles are calculated.[17] We use the following boundary condition during the strain minimization process. The atoms at the top and bottom surfaces of the GaAs cylinder are free to move in any direction. However, to avoid lateral "leakage" of the InAs WL away from cylinder side surface and any resulting unnatural relaxation of the WL along the WL/GaAs interface, we keep fixed the lateral positions of atoms at the cylinder side surface.

A. Tight-binding Hamiltonian diagonalization

In the final step, the tight-binding (TB) Hamiltonian matrix is constructed and the required single-particle states and energies are found. In our TB approach each atom is de-

scribed by its outer valence orbitals for each spin: s, p_x, p_y, p_z and an additional s^* orbital that accounts for higher lying states.[30] Spin-orbit coupling and coupling only of nearest neighbor orbitals is included. Empirical parameters for the unstrained system are obtained by fitting the bulk TB results to experimentally known band gaps and effective masses.[31,32] The valence band offset Δ_v between the InAs and GaAs is taken as 0.2 eV.[33] For the relaxed structure, the TB offsite parameters connecting atoms i and j, V_{ij}, $i \neq j$, have to be recalculated at each atomic site. We use the Slater-Koster formulas[34] to incorporate the effect of changed bond angles on V_{ij} and power-law scaling for the bond lengths $V_{ij}=Vij^0(d_{ij}^0/d_{ij})^\kappa$, where the d_{ij} are the bond lengths and superscript 0 corresponds to the unstrained values. The exponent κ is determined by reproducing experimental values of volume deformation potentials under hydrostatic pressure. The details are given in Ref. 19. The resulting exponent[35] is 2.9. The onsite diagonal TB parameters that represent atomic orbital energies, can also change if the piezoelectric potential, which results from the strained (distorted) lattice, is taken into account. The calculation of the piezoelectric charge follows the procedure described in Ref. 23, while the piezoelectric potential is calculated by numerically solving the Poisson equation on a cubic grid.

More sophisticated tight-binding models could be used with second nearest neighbor coupling or with d atomic orbitals in the basis at considerable additional computational cost. Including d orbitals can be especially important for small quantum dots of GaAs (Ref. 36) where there is a small splitting between side valleys and the zone splitting. In that case, strong quantum confinement can easily mix the side valleys and the zone center states. This splitting is much larger for InAs. Because our bound states are still primarily in the InAs regions, we expect the present tight-binding model to be reasonable. The most important band feature for InAs is the small band gap which leads to strong valence band/conduction band mixing near the zone center gap. Simple tight binding models are defined to reproduce well this part of the band structure. Moreover, due to the coupling between the dots, the quantum confinement effects will be weaker than in isolated dots. Therefore, we expect the tight-binding model we use to give a reasonable representation of systems of strongly coupled dots.

There is no need to perform TB calculations for the huge GaAs buffer used as the VFF domain because electron and hole states trapped in the dots cannot leak out to the edge of the VFF domain. Therefore we cut off a smaller cylindrical domain (the TB domain), which is chosen large enough to ensure that further increases in both horizontal and vertical size do not significantly change the bound state energies and the level ordering. For the single QD, the GaAs cylinder with diameter $24a$ and height $H=16a$ ensures accuracy of a few tens of meV and 2 meV in the calculations of the electron and hole energy levels, respectively. More importantly, differences between the energies of the hole levels change only by a few tenths of meV and the level ordering does not change. The entire relaxed system to be diagonalized contains 77 551 atoms in the case of a single QD and 128 539 atoms[37] in the case of double dots with $d=8a$.

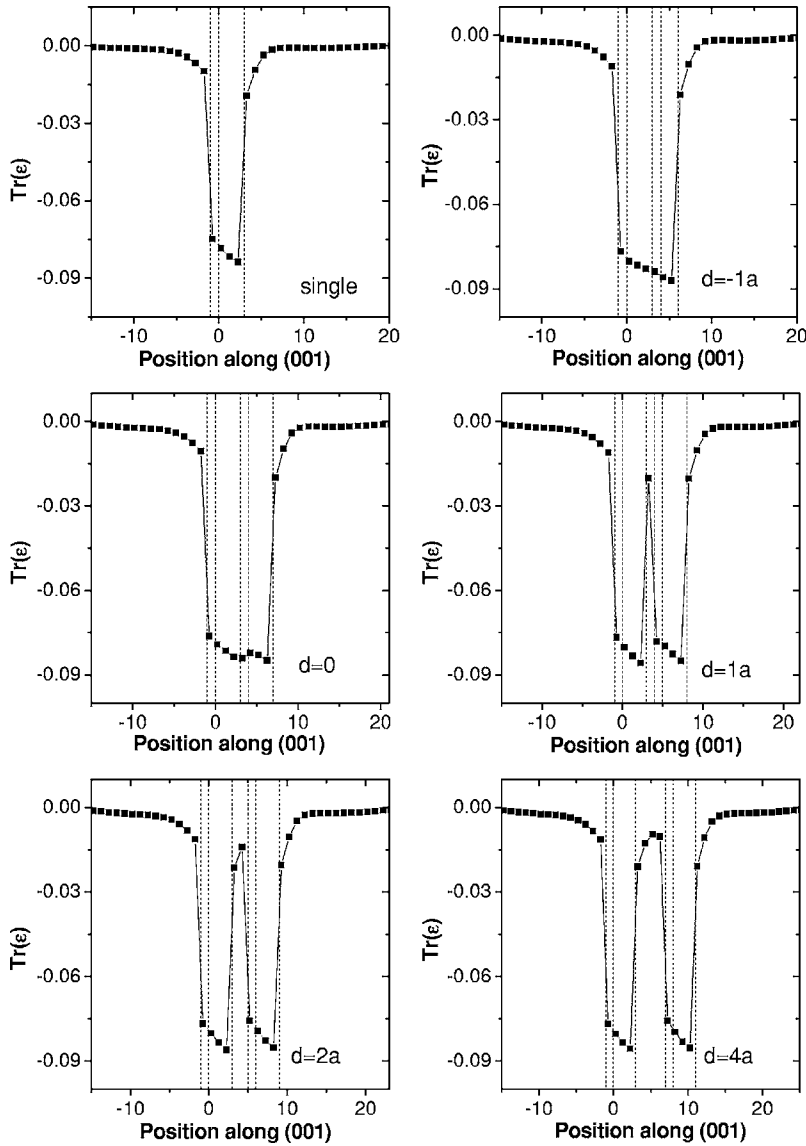Because our TB domain is a cutoff of the VFF domain

FIG. 1. Trace $Tr(\epsilon)$ of the strain tensor vs cation position (in units of lattice constant) along (001), i.e., along z axis, for a single quantum dot and several double quantum dots. Vertical lines mark WLs and tops of QDs.

and is a cylinder with an irregular surface as the result of lattice relaxation, periodic boundary conditions (BC) cannot be used. Instead, we passivate the resulting surface dangling bonds to exclude nonphysical states trapped at the surface of the GaAs cylinder.[21] The passivation is modeled by shifting the energy of these bonds high above the conduction band edge so they do not modify states near the band gap. The eigenvectors of the TB Hamiltonian are found using an iterative solver. Only the electron and hole states with energies close to the InAs conduction and valence band edges are found (usually 50 states).

The single-particle electron-hole transition rates are calculated by evaluating the dipole matrix elements in real space using the TB wave functions. The onsite dipole matrix elements are approximated by the atomic dipole moments,[38] and the dipole moments for nearest neighbors are chosen by reasonable estimates. The details are given in Ref. 30. These rates are used to better identify and confirm state symmetries.

III. RESULTS

A. Strain fields

The trace of the strain tensor, $Tr(\epsilon)$, accounts for the hydrostatic strain. In Fig. 1, $Tr(\epsilon)$ calculated along the (001) direction is shown for a single QD and several double quantum dots separated by $d=-a, 0, a, 2a$, and $4a$ ($d=-a$ means that the lower QD overlaps with the upper WL by a). For all of the cases investigated, almost the entire hydrostatic compressive strain accumulates in the InAs WL and QDs. Even for dots separated by only $d=a$, the GaAs buffer between the dots is almost hydrostatically unstrained. The presence of the second dot modifies negligibly the profile of $Tr(\epsilon)$ for the single QD: its depth increases by $\approx 3\%$. For $d>0$ the $Tr(\epsilon)$ of the lower QD is deeper than the $Tr(\epsilon)$ of the upper dot by less than 1%.

Figure 2 shows the biaxial component of strain defined as $B=\epsilon_{zz}-(\epsilon_{xx}+\epsilon_{yy})/2$. For $d>0$, the GaAs layer separating the dots becomes strongly biaxially strained. The biaxial component is positive in the InAs WL and QDs and negative in the
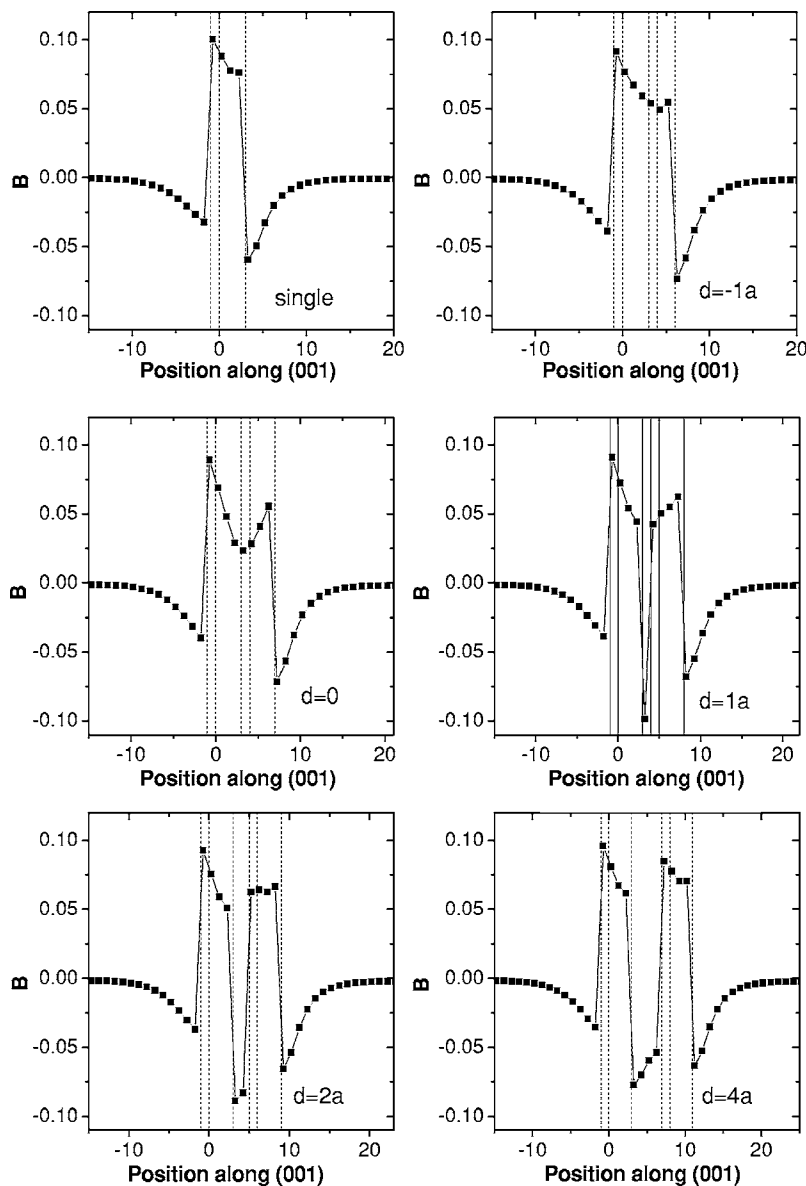
FIG. 2. Biaxial component B of the strain tensor vs cation position (in units of lattice constant) along (001) for a single quantum dot and several double quantum dots. Vertical lines mark WLs and tops of QDs.

GaAs layer separating the dots. The maximum absolute value of the biaxial strain in this GaAs layer is almost the same as in the quantum dots.

For $d=8a$ (not shown), the largest $|B|$ in GaAs is 10% greater than the largest $|B|$ in GaAs for the single QD. Because the biaxial component of strain affects mainly the valence band states[17] we expect enhanced mixing of the valence subbands for closely spaced dots caused by the strong biaxial strain in the intermediate GaAs layer. Additionally, for $d<8a$, B in the lower dot is significantly larger than in the upper QD. This strain asymmetry, reported previously in Ref. 18 for truncated pyramidal dots, promotes stronger localization of the ground hole state in the lower dot.

Although TB calculations include strain effects directly via modification of the offsite parameters, the strain tensor elements and deformation potentials[17] can still be used to estimate strain-induced confinement potentials for the electrons and holes. In Fig. 3 the conduction (CB), heavy hole (HH), light hole (LH), and split-off (SO) band profiles along (001) direction are shown and are compared to the bulk un-strained GaAs/InAs band offsets. The biaxial strain component, responsible for the heavy-hole and light-hole splitting, has the opposite sign in InAs and GaAs, yielding a reversal of the HH-LH splitting between the materials. As a consequence, strain effects enhance the HH well in the InAs regions and the HH barrier in the GaAs separating layer. Simultaneously, the strain weakens the light-hole well in the InAs regions and the light-hole barrier in the GaAs regions. For small d, the effect is so strong that it leads to the formation of a light-hole well in the GaAs separating layer that is even deeper than the corresponding well in the InAs quantum dots. This effect was reported for truncated pyramids in Ref. 18. Here, we show that for small lenses the deep LH GaAs well survives even up to $d=8a$ (≈ 7 nm separation between the quantum dot centers).

B. Electronic structure

The dependence of the lowest electron and hole energy levels of DQDs on separation distance are shown in Figs. 4
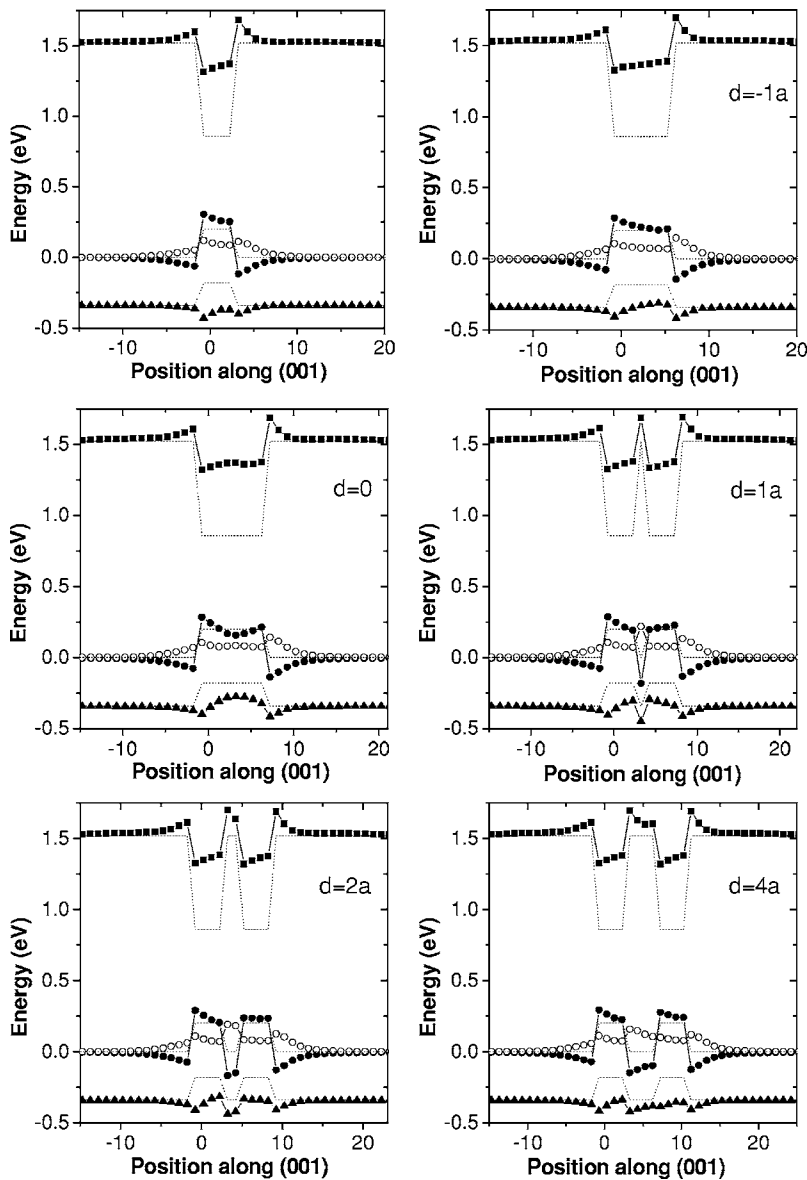
FIG. 3. Strain-induced confining potentials for a single quantum dot and several double quantum dots vs cation position (in units of lattice constant) along (001). CB—squares, HH—closed circles, LH—open circles, SO band—triangles, bulk unstrained GaAs/InAs band offsets—dotted lines.

and 5, respectively. Energy levels found with (upper panels) and without (lower panels) strain are shown. The energies are shown relative to the top of the GaAs valence band. The hole energies are shown as the energies of valence electrons (i.e., with the hole ground state having the highest energy shown). The corresponding state densities are presented in Figs. 6 and 7. For $d>2a$ the two lowest electron energy levels correspond to bonding and antibonding states built from the ground states of the single dots with the bonding state being lower in energy, as expected. Similarly, p-type states show a bonding/antibonding hybridization in DQDs with the bonding states at lower energy. The density of the lowest electron bonding state is almost equally distributed in both dots. When the strain effects are taken into account, the antibonding state localizes more in the lower dot. This is due to the asymmetry of the strain-modified CB confining potential well (seen in Fig. 3), which affects more the excited states. Strain makes the InAs CB potential wells shallower, enhances the coupling between the dots, and therefore increases the energy splitting between bonding and antibond-

ing states. This is especially well seen in the case of the pair of p-type states. Strain enhances also the energy splitting between the two perpendicularly polarized p-type states of a single QD, known as *atomistic interface effect* (described in detail in Refs. 39 and 41). Moreover, strain pushes the crossing of the electron energy levels of different symmetries to higher d.

Because the single QD has only one electron state fully bound and localized in the quantum dot, the DQD should in principle possess two bound states. This is the case for $d>2a$. However, for $d<a$ only one electron state is bound in the DQD. For $d=a$ and $d=2a$ one can observe (Fig. 6) an exotic sequence of the energy levels: the excited state built of s-type ground states of single dots, lies above the WL continuum edge,[42] although this state is bound and localized in the QD regions. This happens because the *bondinglike* combinations of the p-type states for single dots (which form the WL continuum edge) decrease their energies for decreasing d and for small d drop below the first excited s-type state, which is still localized in the QD regions and has to be con-
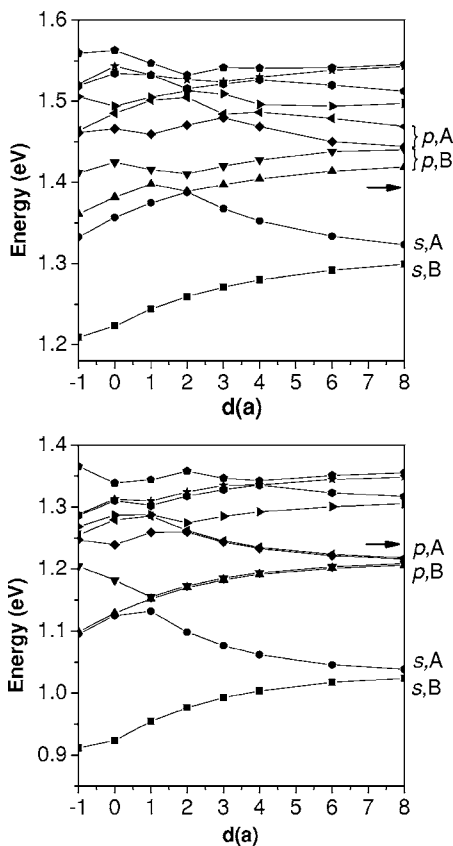
FIG. 4. Dependence of the lowest electron energy levels of a DQD on separation distance d in units of lattice constant. Top—strain effects included, bottom—without strain effects. The arrows mark the WL quasicontinuum of a single QD. Energies are referred to the bulk GaAs valence band edge. The state character (s,p) for widely spaced dots is indicated; B—bonding, A—antibonding. Lines connect and order states energetically. Changing character of states after crossing points can be recognized from density plots (Fig. 6).

FIG. 5. Dependence of the lowest hole energy levels of a DQD on separation distance d in units of lattice constant. Top—strain effects included, bottom—without strain effects. The arrows mark the WL quasicontinuum of a single QD. Energies are referred to the bulk GaAs valence band edge. Lines connect and order states energetically. Dotted lines show how some states would evolve vs d in the absence of mixing.

sidered a bound state of the DQD. Such a situation is allowed because the s-type state does not couple to the p-type WL continuum. This state will further delocalize for decreasing d when it reaches the *bondinglike* WL continuum of the same symmetry.

Considering the hole states when the strain effects are not taken into account (Fig. 5 bottom), the ground hole state (highest valence band level) is pushed monotonically to higher energies with decreasing d (its energy splitting from the InAs valence band edge at 0.2 eV decreases). When strain is included (Fig. 5 top), the ground hole state is pushed to lower energy as d decreases down to $d \approx a$ (its energy splittng from the InAs valence band edge increases). However, for even smaller separation distances, $d < a$, the ground hole state is pushed to higher energy (its energy splitting from the InAs valence band edge decreases). This surprising nonmonotonic behavior with distance confirms the results of calculations performed in Refs. 9 and 25 in the framework of pseudopotential approach. Comparison of the results presented in both panels of Fig. 5 proves that this effect for $d > a$ is a direct consequence of strain. Associated with the observed dependence of the ground hole state energy on d
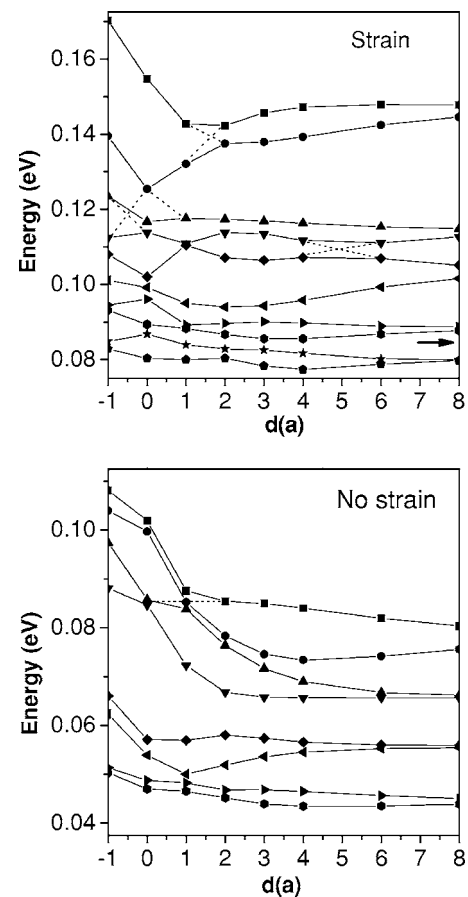
for strained dots is its stronger localization in the lower dot for $d=0$ and $d=a$ (Fig. 7). However, one should note that for these d the density of the ground hole state in the upper dot is not zero (although it is not visible within the isosurface containing 50% of the density around the density maximum).

Bester, Zunger, and Shumway [25] explained this effect of the strain on the hole state localization by (i) the existence of a high HH barrier in the GaAs interdot region and (ii) the asymmetry (the lack of inversion symmetry) between the dots. The asymmetry can also explain why, for a range of d, the first two hole states increase their energies (relative to the InAs valence band edge) for decreasing d (unlike the lowest two bonding electron states). A closer inspection of Fig. 3 shows that the HH-well asymmetry is mainly due to the shallower well in the upper dot: for $d < 4a$ the upper HH well becomes as shallow and flat as the unstrained well, while the HH well in the lower dot is always deeper and is almost insensitive to the variation of d (its depth and shape are always similar to the HH well of the dot). This observation on the behavior of the double HH well versus separation distance explains why the binding energy of the ground hole state decreases and this state localizes in the lower dot for
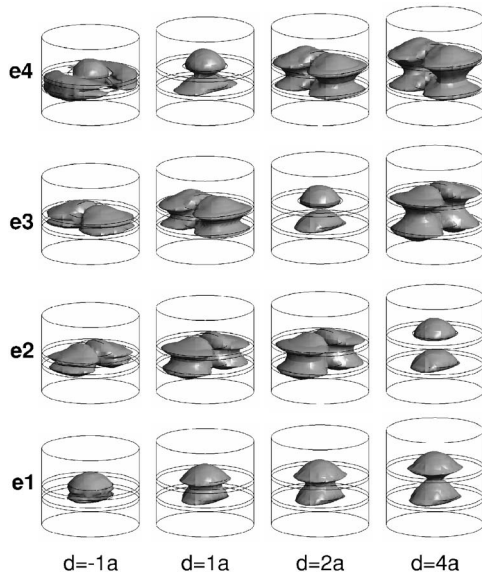
FIG. 6. Density isosurfaces (50%) of the four lowest electron states in a DQD versus separation distance d. Internal circles mark the positions of the WLs. The outermost cylinder marks the size of GaAs buffer. Strain effects are included. The diffused states have energies in the WL continuum.

decreasing d. In contrast to the results of pseudopotential calculations,[25] our TB model predicts weaker localization of the ground hole state in the lower dot (and thus weaker localization of the first excited state in the upper dot) at large separation distances.
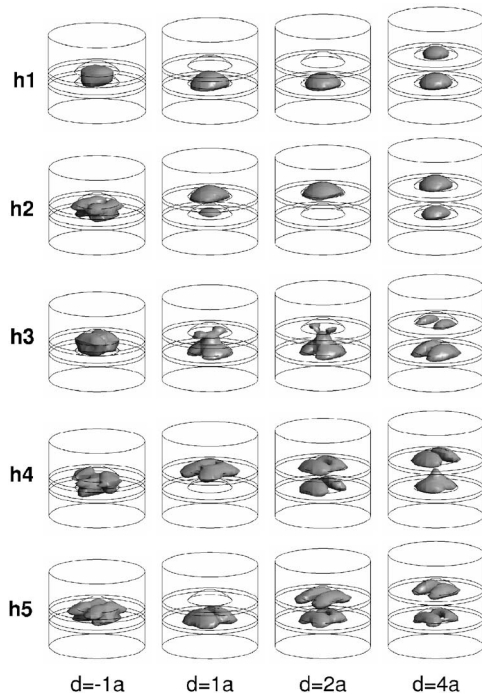

FIG. 7. Density isosurfaces (50%) of the five bound hole states in a DQD versus separation distance d. Strain effects are included. Internal circles mark the positions of the WLs. The outlines of the QDs are indicated.

In our previous work[43] we showed that, in the absence of strain effects, the first two hole states of the DQD have well-defined bonding or antibonding character. Most importantly, for large separations, the ground hole state in the DQD has antibonding character, rather than the usual bonding character, with the next higher hole state being a bonding state. This unusual ordering is reversed, returning to the usual ordering with a more bondinglike ground state for small separations, as will be evidenced latter in our calculations of optical transitions. The same unusual ordering for large d is seen when the strain is included.

To understand this unusual ordering at large d, one can consider Fig. 8, which shows the spatial envelope for different components of the hole ground state and first excited state along the (001) direction through the point $x=0.5a$, $y=2a$. The p_x and p_y atomic orbital components have a spatial envelope with even z parity inside the single dot, while the p_z atomic orbital component has a spatial envelope with odd z-parity inside the dot [see Fig. 8(a)]. Although the p_z atomic orbital contribution to the ground state is smaller because it is LH-like, it extends further from the dot (in regions not shown in the figure) because it is LH-like. Thus, for widely spaced dots [Fig. 8(b)], the coupling in the DQD is through the p_z component, which can be dominant in the region between the two dots. As shown in Fig. 8(b), a normal bonding is expected if the coupling is via the p_x and p_y components which are large inside the dots. However, when the coupling is via the p_z component, charge buildup between the dots via the p_z component requires an antibonding configuration. Figures 8(c) and 8(d) confirm that the ground hole state in widely spaced DQDs is antibonding in both strained and unstrained structures. As shown in Figs. 8(e) and 8(f), the next higher hole state has the bonding character in widely spaced DQDs.

The p_x and p_z contributions for the first two hole states of a DQD with strain included [Figs. 8(d) and 8(f)] are almost the same as when strain effects are not taken into account [Figs. 8(c) and 8(e)]. As a consequence, for $d>2a$ the first two hole states of the DQD have well-defined character of bonding- and antibondinglike "molecular" states. This is also true for smaller d, although for $d=a$ and $d=2a$ the 50% isosurfaces do not show densities in one of the dots. When we analyze the electron-hole transition rates, we will show that although the ground hole state prefers to localize more in the lower dot, the entire wave function still preserves the bonding or antibonding molecular character, even for $d=0$ and $d=a$ as defined by the parity-allowed transitions.

Figures 5 and 7 demonstrate that higher hole states of the DQD undergo a complex evolution for varying d caused by the long-range strain effects. In particular, the fourth and fifth states cross when d decreases from $6a$ to $4a$. The corresponding energy levels cross again at $d=a$. For $d=0$ and $d=-a$ the first excited hole state is the one that originates from the third hole state at $d=8a$. At $d=-a$, the in-plane (x,y) symmetries of the first three hole states evolve to the first hole states of the single QD. We also observe (Fig. 7) that higher hole states can also localize to one dot or the other for some d. This is especially well seen for $d=a$.
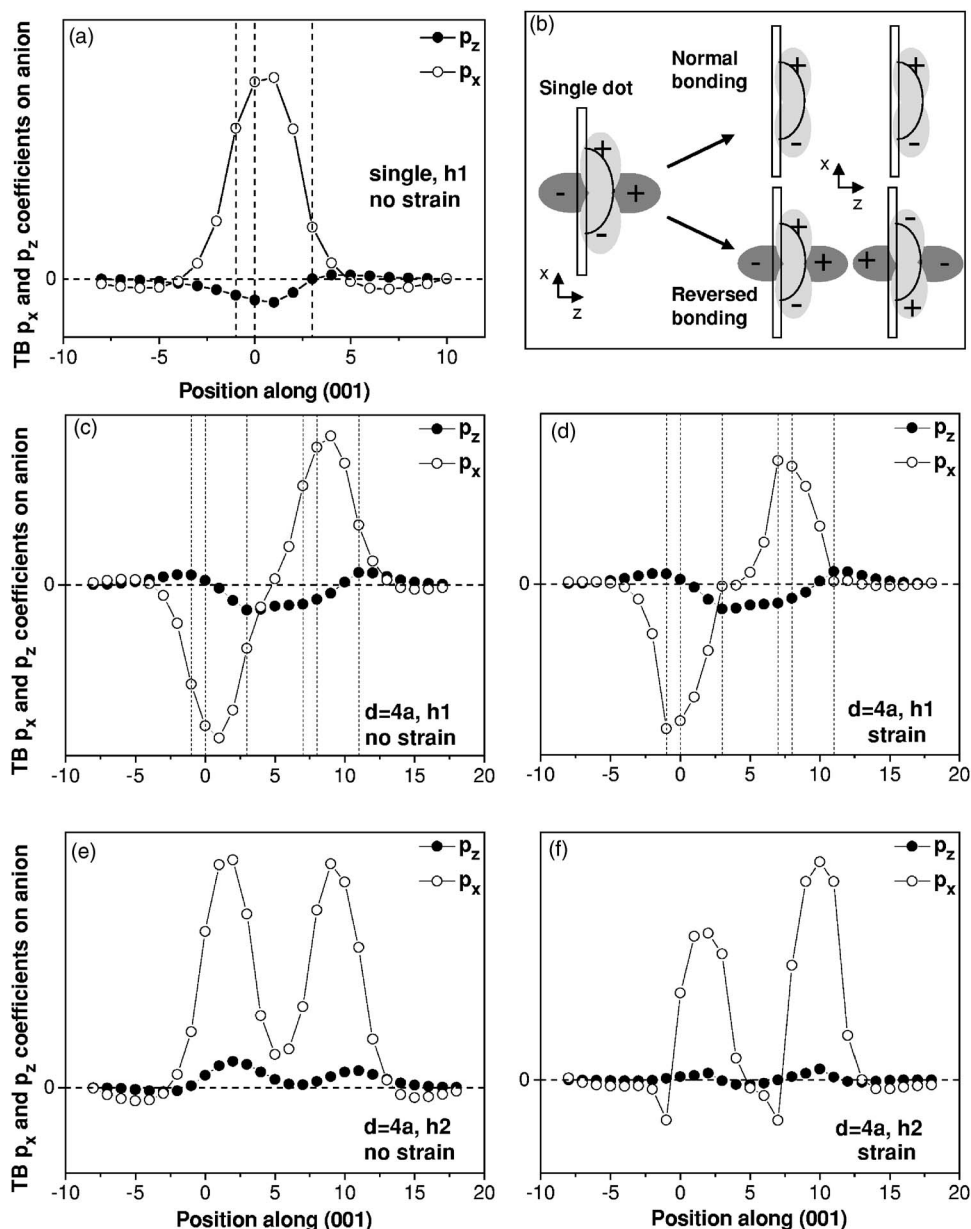
FIG. 8. Spatial envelopes of the p_x and p_z atomic orbital contributions to hole wave functions along (001) at $x=0.5a$, $y=2a$: (a) Single QD ground hole state, (c) DQD ($d=4a$) ground hole state h1, no strain effects, (d) DQD ($d=4a$) ground hole state h1 with strain effects, (e) DQD ($d=4a$) first excited hole state h2, no strain effects, (f) DQD ($d=4a$) first excited hole state h2 with strain effects. Full circles indicate p_z contribution, open circles, p_x contributions, respectively. Vertical lines in (a) indicate the wetting layer and the top of the quantum dot. Vertical lines in (c) and (d) indicate the wetting layers and the top of the dots in the DQD. Similar lines should apply for (e) and (f). (b) A scheme showing normal and reverse bonding of the QDs ground hole states.

C. Piezoelectric effect

We have also studied the piezoelectric effect in DQDs. Recently, Bester and Zunger showed[39] that the piezoelectric effect may be comparable to the strain and atomistic interface effects in large enough quantum dots. They showed that inclusion of the piezoelectric effect can change the polarization of the pair of *p*-like electron states in a single quantum dot. The quantum dots investigated in our paper are smaller than the dots studied in Ref. 39. Because piezoelectric effects are proportional to the size of the QD (to the size of the strained region), the influence of piezoelectric effects on the energy structure and charge densities of the dots investigated here is negligible. In particular, the energies of the ground electron and hole state of the single QD change by 1 and 2 meV, respectively; the splitting between the *p*-type electron energy levels changes by only 2 meV. For DQDs, the effects are even smaller. To understand why the piezoelectric

effect decreases for double quantum dots, even though the size of the strained region increases, we have analyzed the piezoelectric potential versus distance between the dots, as shown in Fig. 9. Although the piezoelectric potential increases below the lower dot and above the upper dot, the potential largely cancels between the dots. This effect is partially present even for $d=12a$. The partial cancellation of this potential is due to its quadruple character and its odd parity in the z direction.

The piezoelectric effect is negligible in the case of the QDs studied here. Moreover, recent results presented in Ref. 40 show that when the second order contribution to the piezoelectric field is taken into account, the quadratic terms yield further significant reduction of the piezoelectric effect.

D. Optical rates

Finally, we study the single-particle optical spectra of double quantum dots to better understand the electron and
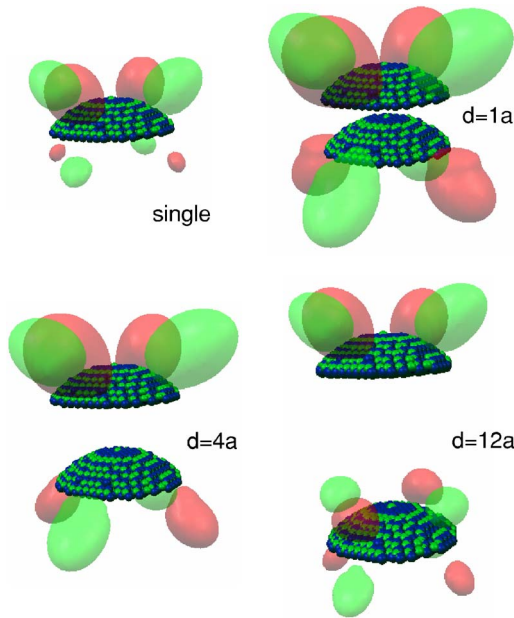
FIG. 9. (Color online) Piezoelectric potential for single and several double quantum dots. Isosurfaces of 10 meV. (Colors): red—positive, green—negative potential. Blue and green dots mark the In and As atoms in the QDs.

hole state symmetries. Near-band-edge transition rates for several DQDs versus distance d are shown in Fig. 10. For comparison, transition rates for a single QD (i.e., for two very widely spaced dots) are also shown. The transition rates are averaged over x, y, and z polarizations. For $d > a$, the transition between the ground electron and hole states ($e1$-$h1$) is forbidden by parity. The same happens for the transition between $e2$ and $h2$. The first pair of optically active transitions are $e1$-$h2$ and $e2$-$h1$. Because the lowest electron state always has bondinglike character, this shows that for $d = 3a, 4a$ and larger separations the ground hole state of DQD is largely antibonding (although not equally distrib-
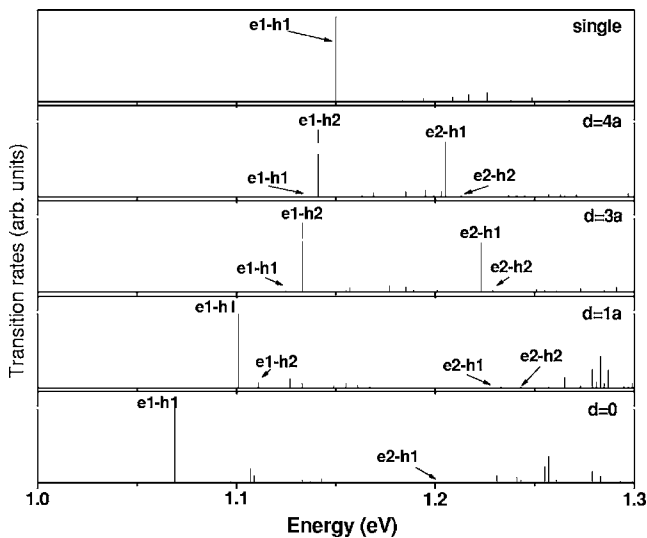

FIG. 10. Electron-hole transition rates for single and several double quantum dots versus separation distance d.

uted in the dots, see Fig. 7). For $d = a$ the $e1$-$h1$ transition becomes optically active, showing that for $d = a$ the ground hole state of the DQD is a bondinglike combination of the ground hole states of single dots (although the 50% isosurface in Fig. 7 shows a very asymmetric distribution of the density between both dots). One observes also a negligible rate for the $e2$-$h2$ transition for small separation distance between the dots. This is because the p-type electron state ($e2$) becomes the first excited state for $d < 3a$ (see Figs. 4 and 6).

Fafard and co-workers investigated the photoluminescence of vertically stacked double InAs quantum dots versus distance between dots.[14] The smallest dots studied in Ref. 14 had heights close to 2 nm ($\approx 3.5a$). In Ref. 14 they observed a 23 meV redshift for the lowest transition when the distance d_c between the dot centers decreased from 15 to 4 nm. The distance $d_c = 15$ nm corresponds to $d \approx 23a$ and means practically noninteracting dots, effectively two single dots. $d_c = 4$ nm corresponds to $d \approx 3.5a$. This qualitative agreement is, at best, suggestive. A full calculation including the electron-hole binding and its effect on the transition rates would be needed for a full comparison. However, we expect the measured splitting between widely spaced levels (i.e., the electron levels) to be more directly given by the single-particle splittings because these levels are not so strongly mixed by the electron-hole interaction. The calculated redshifts for $d = 3a$ and $d = 4a$ are equal to 25 and 18 meV, respectively and corresponds well with the experimental value of 23 meV. The calculated energy splitting between the lowest electron states, $e1$ and $e2$, is 72 meV for separation distance $d = 4a$. This splitting agrees well with the measured energy splitting between the two lowest electron energy levels of 70 meV.

IV. SUMMARY

We have used an empirical tight-binding theory to study electronic and optical properties of double InAs/GaAs self-assembled vertically stacked quantum dots. The dots are lens shaped and are situated on 2 ML thick wetting layers. We have investigated strongly coupled systems, allowing even for the partial overlap of the lower QD and the upper WL. For closely spaced dots, our TB VFF calculations confirm the strain-induced tendency of the ground hole state to localize in the lower dot, as predicted previously by multiband **kp** (Ref. 18) and pseudopotential[25] approaches. However, for the sizes and shapes of dots investigated here, the TB calculations predict weaker localization at large separation distances. We have shown how the energy levels evolve with decreasing distance between the dots and how their ordering and symmetries change for very closely spaced and overlapping systems. In particular, for small separation distances, we demonstrated the existence of localized electron states (built as the *antibonding* combination of the ground states of single dots) with energies above the WL continuum edge. For large separation distances, the ground hole state of a DQD has an antibonding character that changes to bonding-

like for $d < 2a$. This effect, predicted previously for unstrained dots, is present also for strongly strained systems. Our calculations have revealed that the bonding/antibonding character of the first two hole states is maintained even for small d, although most of the density is localized in one of the dots. For very small d ($d < a$) no localization is observed. Finally, the calculated redshift of the lowest electron-hole transition for decreasing distance between the interacting dots agrees qualitatively with the experimentally measured redshift for coupled dots of similar sizes and shapes.

*Present address: Institute for Microstructural Sciences, National Research Council of Canada, 1200 Montreal Road, Ottawa, Ontario K1A 0R6, Canada.

[1] A. P. Alivisatos, Science **271**, 933 (1996).

[2] C. R. Kagan, C. B. Murray, M. Nirmal, and M. G. Bawendi, Phys. Rev. Lett. **76**, 1517 (1996).

[3] H. Dollefeld, H. Weller, and A. Eyuchmuller, Nano Lett. **1**, 267 (2001).

[4] V. G. van der Weil, S. De Franceschi, J. M. Elzerman, T. Fujisawa, and L. P. Kouvenhoven, Rev. Mod. Phys. **75**, 1 (2003).

[5] W. J. M. Naber, T. Fujisawa, H. W. Liu, and W. G. van der Wiel, Phys. Rev. Lett. **96**, 136807 (2006).

[6] D. Bimberg, M. Grundmann, and N. N. Ledentsov, *Quantum Dot Heterostructures* (Wiley, New York, 1999).

[7] M. Grundmann, Physica E (Amsterdam) **5**, 167 (1999).

[8] I. Shtrichman, C. Metzner, B. D. Gerardot, W. V. Schoenfeld, and P. M. Petroff, Phys. Rev. B **65**, 081303(R) (2002).

[9] G. Bester, J. Shumway, and A. Zunger, Phys. Rev. Lett. **93**, 047401 (2004).

[10] M. Bayer, *et al.*, Science **291**, 451 (2001).

[11] M. Korkusinski and P. Hawrylak, Phys. Rev. B **63**, 195311 (2001).

[12] G. W. Bryant and G. S. Solomon, *Optics of Quantum Dots and Wires* (Artech House, Boston, 2005).

[13] M. V. Artemyev, A. I. Bibik, L. I. Gurinovich, S. V. Gaponenko, and U. Woggon, Phys. Rev. B **60**, 1504 (1999).

[14] S. Fafard, M. Spanner, J. P. McCaffrey, and Z. R. Wasilewski, Appl. Phys. Lett. **76**, 2268 (2000).

[15] G. S. Solomon, J. A. Trezza, A. F. Marshall, and J. S. Harris, Jr., Phys. Rev. Lett. **76**, 952 (1996).

[16] O. Stier, M. Grundmann, and D. Bimberg, Phys. Rev. B **59**, 5688 (1999).

[17] C. Pryor, J. Kim, L. W. Wang, A. J. Williamson, and A. Zunger, J. Appl. Phys. **83**, 2548 (1998).

[18] W. Sheng and J.-P. Leburton, Appl. Phys. Lett. **81**, 4449 (2002).

[19] R. Santoprete, B. Koiller, R. B. Capaz, P. Kratzer, Q. K. K. Liu, and M. Scheffler, Phys. Rev. B **68**, 235311 (2003).

[20] J. Kim, L. W. Wang, and A. Zunger, Phys. Rev. B **57**, R9408 (1998); L. W. Wang, J. Kim, and A. Zunger, *ibid.* **59**, 5678 (1999); L. W. Wang and A. Zunger, *ibid.* **59**, 15806 (1999); A. J. Williamson, L. W. Wang, and A. Zunger, *ibid.* **62**, 12963 (2000).

[21] S. Lee, F. Oyafuso, P. von Allmen, and G. Klimeck, Phys. Rev. B **69**, 045316 (2004).

[22] S. Lee, O. L. Lazarenkova, P. von Allmen, F. Oyafuso, and G. Klimeck, Phys. Rev. B **70**, 125307 (2004).

[23] T. Saito and Y. Arakawa, Physica E (Amsterdam) **15**, 169 (2002).

[24] W. Sheng and J. P. Leburton, Phys. Rev. Lett. **88**, 167401 (2002); J. J. Palacios and P. Hawrylak, Phys. Rev. B **51**, 1769 (1995); B. Szafran, S. Bednarek, and J. Adamowski, *ibid.* **64**, 125301 (2001); A. Schliwa, O. Stier, R. Heitz, M. Grundmann, and D. Bimberg, Phys. Status Solidi B **224**, 405 (2001); L. R. C. Fonseca, J. L. Jimenez, and J. P. Leburton, Phys. Rev. B **58**, 9955 (1998); M. Korkusiński and P. Hawrylak, *ibid.* **63**, 195311 (2001); S. Taddei *et al.*, Phys. Status Solidi B **224**, 413 (2001); A. Vasanelli, M. De Giorgi, R. Ferreira, R. Cingolani, and G. Bastard, Physica E (Amsterdam) **11**, 41 (2001); M. Tadić, F. M. Peeters, B. Partoens, and K. L. Janssens, *ibid.* **13**, 237 (2002).

[25] G. Bester, A. Zunger, and J. Shumway, Phys. Rev. B **71**, 075325 (2005).

[26] L. He, G. Bester, and A. Zunger, Phys. Rev. B **72**, 081311(R) (2005).

[27] T. Hanada and T. Yao, Microelectron. J. **36**, 216 (2005).

[28] We have checked that the final results and conclusions are essentially independent of the choice of QD base center position. Also, choosing the WL thickness to be 1 ML does not significantly change the results.

[29] W. H. Press, B. R. Flannery, S. A. Teukolsky, and W. T. Vettering, *Numerical Recipies* (Cambridge University Press, Cambridge, 1988).

[30] G. W. Bryant and W. Jaskólski, Phys. Rev. B **67**, 205320 (2003).

[31] G. Klimeck, R. C. Bowen, T. B. Boykin, and T. A. Cwik, Superlattices Microstruct. **27**, 519 (2000).

[32] The onsite energies defined by Klimeck for GaAs (Ref. 31) have an order opposite to the common ordering of these energy levels with the levels of Ga and As in reverse order. This produces conduction band states that are primarily located on the anions and vice versa. We reverse the ordering of these levels to obtain conduction (valence) band states located primarily on the cations (anions). This can be done without significantly altering the predicted GaAs zone center bulk band structure.

[33] The influence of the valence band offset Δ_v on the QD effective gap was studied in Ref. 19. No significant influence was found for Δ_v in the wide range of experimental values 0.05–0.3 eV. Therefore, we use a value in the middle of the experimental range.

[34] J. C. Slater and G. F. Koster, Phys. Rev. **94**, 1498 (1954).

[35] A different value of κ was obtained in Ref. 19 due to different TB parametrization (s, p^3, d^5, s^*).

[36] J. G. Diaz and G. W. Bryant, Phys. Rev. B **73**, 075329 (2006).

[37] In similar calculations performed by Santoprete *et al.* (Ref. 19), for pyramidal QD of the base lengths 12a and height 6a, a GaAs

box of dimensions $25a \times 25a \times 17a$ was used (85 000 atoms) to get the stability of the effective gap to the level of a few meV.

[38] S. Fraga and J. Muszyńska, *Atoms in External Fields* (Elsevier, New York, 1981).

[39] G. Bester and A. Zunger, Phys. Rev. B **71**, 045318 (2005).

[40] G. Bester, X. Wu, D. Vanderbilt, and A. Zunger, Phys. Rev. Lett. **96**, 187602 (2006).

[41] M. Zielinski, W. Jaskólski, J. Aizpurua, and G. W. Bryant, Acta Phys. Pol. A **108**, 929 (2005).

[42] The WL continuum is discretized in our calculations.

[43] W. Jaskólski, M. Zieliński, and G. W. Bryant, Acta Phys. Pol. A **106**, 193 (2004).